

Polarization in fragmentation, g factor of ^{35}K

M. Schäfer,* W.-D. Schmidt-Ott, T. Dörfler, T. Hild, and T. Pfeiffer
II. Physikalisches Institut, Universität Göttingen, D-37073 Göttingen, Germany

R. Collatz,† H. Geissel, M. Hellström, Z. Hu, H. Irnich, N. Iwasa,‡ M. Pfützner, E. Roeckl, and M. Shibata§
GSI-Darmstadt, D-64291 Darmstadt, Germany

B. Pfeiffer
Institut für Kernchemie, Universität Mainz, D-55099 Mainz, Germany

K. Asahi, H. Izumi,|| H. Ogawa, and H. Sato¶
Tokyo Institute of Technology, Meguro-ku, Tokyo 152, Japan

H. Ueno
Department of Physics, Osaka University, Toyonaka, Osaka 560, Japan

H. Okuno
The Institute of Physical and Chemical Research (RIKEN), Wako-shi, Saitama 351-01, Japan

(Received 26 August 1997)

Spin polarization $P > 1\%$ has been observed for ^{37}K fragments produced in the reaction $^{40}\text{Ca} + ^9\text{Be}$ at 500 MeV/nucleon. The polarization was measured as a function of fragment longitudinal momentum (Goldhaber distribution). The experimental results are well described by a new Monte Carlo-based model. The β -decay half-life of ^{35}K was remeasured as $t_{1/2} = 178(8)$ ms. Using polarized ^{35}K fragments, the g factor $g_{\text{exp}}(^{35}\text{K}) = 0.24(2)$ was measured. The magnetic moments of isospin $|T_z| = 3/2$ mirror pairs are discussed. [S0556-2813(98)03305-6]

PACS number(s): 25.70.Mn, 29.27.Hj, 21.10.Ky, 27.30.+t

I. INTRODUCTION

Products of fragmentationlike reactions at Fermi energies are known to be spin polarized [1]. This feature has been ascribed to a recoil of the nucleons removed peripherally from the localized volume of the projectile. The experimental data indicate that for any specific (small) deflection angle, a distinction can be made between the near- and far-side (right and left) trajectories of the projectile around the target nucleus [1,2]. A small contribution to the fragment polarization of another mechanism as proposed by Okuno *et al.* [2] was also identified. It is based on the assumption that the abraded nucleons are more likely to be removed from the backward hemisphere of the projectile with respect to the

projectile beam direction. In the low- and medium-energy range, the polarization of projectile fragments was successfully applied to g -factor measurements of unstable nuclei via β -nuclear magnetic resonance (NMR) spectroscopy [1,3,4].

In the relativistic energy domain, where the deflection of fragments due to Coulomb and nuclear forces is much smaller than the angular straggling induced by the (intrinsic) transverse momentum of the removed nucleons, no distinction between near and far trajectories can be made. Consequently, no polarization of the fragments due to the mechanism dominating at Fermi energies is predicted. Only the alignment of fragment spins is likely to occur at the very high projectile energies and was recently measured at the GSI-Darmstadt. In that experiment [5], the spin alignment of ^{43m}Sc fragments was detected because of the anisotropy of emitted γ rays using the time differential perturbed angular correlation (TDPAC) method.

On the other hand, the second mechanism based on the forward/backward asymmetry in the abrasion of nucleons could produce spin polarization also at higher energies. The aim of this work was to check this hypothesis.

In a recent experiment, the fragment separator (FRS) was used to produce and separate such fragments for an investigation of their polarization by the β -NMR method. Preliminary results were already reported in [6]. In addition, the implications of the ^{35}K result for the magnetic moment systematics of isospin $= 1/2$ and $3/2$ mirror nuclei pairs are discussed, as well as a new Monte Carlo-based model describing the mechanism behind polarization in fragmentation

*Present address: Roland Berger & Partner GmbH, International Management Consultants, Arabellastraße 33, 81925 München, Germany.

†Present address: EG&G GmbH, Verkaufsbüro Berlin, D-14197 Berlin, Germany.

‡Present address: Department of Physics, Osaka University, Toyonaka, Osaka 560, Japan.

§On leave from: School of Engineering, Nagoya University, Chigusa-ku, Nagoya 464-01, Japan.

||Present address: Department of Physics, Osaka University, Toyonaka, Osaka 560, Japan.

¶Present address: The Institute of Physical and Chemical Research (RIKEN), Saitama 351-01, Japan.

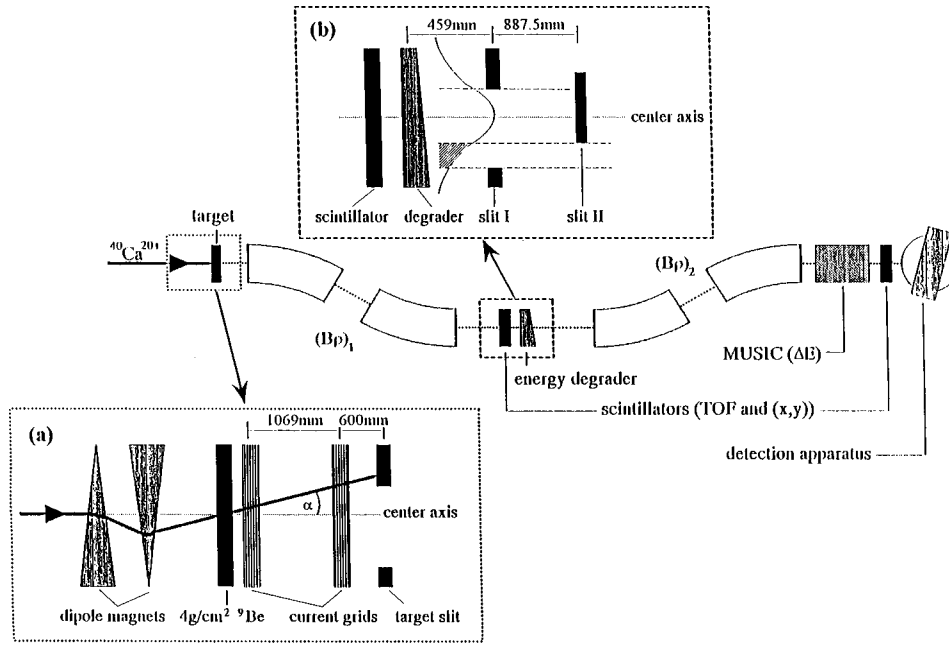


FIG. 1. Fragment separator FRS at GSI and stopping area. Insert (a): tilted beam on target (viewed from above). Insert (b): new slit system in the dispersion plane (viewed from above) for selection of a longitudinal momentum cut; each jaw of slit I can be moved in the x direction up to center, slit II is movable in the x direction across the center axis of FRS.

reactions at high energies. This paper deals with the experiment in detail, including the positive identification of polarization of $^{35,37}\text{K}$ and the application of polarization to a first measurement of the ^{35}K g factor.

II. EXPERIMENTAL PROCEDURE

The nuclides studied were produced from fragmentation of a 500 MeV/nucleon ^{40}Ca beam delivered by the GSI synchrotron SIS in a 4 g/cm^2 ^9Be target placed at the entrance of the projectile fragment separator FRS [7] (see Fig. 1). The average intensity was 10^8 particles per spill, with 3 seconds between consecutive spills. The extraction time was adjusted according to the half-lives of the nuclides under investigation. The angle of the incident beam could be adjusted in the range ± 10 mrad using two dipole magnets upstream of the target [see insert (a) of Fig. 1]. The fragments were separated in the FRS and identified using standard energy loss vs time-of-flight techniques. The right or left side of the fragment transverse momentum distribution could be selected with slits placed directly after the target. An additional selection across the fragment longitudinal momentum (Goldhaber (GH) distribution) was achieved with new slits placed at the middle dispersive plane of the FRS. With these slits, any part of the GH distribution can quickly be selected without retuning of the FRS [see insert (b) in Fig. 1].

At the final focal plane of the FRS, angle- and momentum-selected ^{39}Ca and $^{35,37}\text{K}$ fragments were slowed down in an aluminum degrader before being implanted into a stopper crystal placed in the central region of a room-temperature magnet (see Fig. 2). The self-constructed 33000-ampere-turn magnet with an 82 mm pole gap was used to produce a strong static magnetic field B_0 . The long-term constancy of the field was monitored with a Hall probe. The stability of the field, achieved by using temperature-

controlled oil cooling, was better than 0.2% at $B_0=0.493\text{ T}$, while the field inhomogeneity across the implantation crystal was less than 1%.

The stopper consisted of a $30\text{ mm}\times 60\text{ mm}\times 3\text{ mm}$ single-crystal, either CaF_2 or KBr , tilted at an angle of 30° with respect to the beam axis. In previous experiments, ionic crystals had been used for stopping Ca and K isotopes. A large percentage of the original spin polarization is preserved in ion implantation into crystals containing the same kind of positive ions [8,9]. Depolarization effects due to spin-lattice relaxation are small. At room temperature ($T=293\text{ K}$), experimental relaxation times were several seconds [8,9], and are thus much longer than the half-lives of the investigated nuclei. The polarization produced in the fragmentation reaction is expected to be preserved during the deceleration of the ions in the target and degrader materials and is maintained after implantation in the static magnetic field.

With the help of two Si detectors in front of and one PIN-diode behind the stopper, the implantation profile was optimized by adjusting the thickness of the degrader (see Fig. 2). Two $120\text{ mm}\times 100\text{ mm}$ scintillator telescopes were placed above and below the center of the stopper crystal, each telescope covering a solid angle of 32%. The telescopes consisted of one 1.5-mm-thick and two 3-mm-thick plastic scintillators, the latter separated by a 6 mm aluminum layer (see Fig. 2). Using glass fibers, the scintillators were optically coupled to photomultiplier (PM) tubes placed outside the static magnetic field.

The telescopes allowed to measure the up-to-down ratios of positrons emitted in the decay of the implanted fragments. In order to compensate for geometrical asymmetries of the setup and to determine the nuclear magnetic resonance, the spin-reversal produced in an adiabatic fast passage (AFP) of the magnetic moments in a radio frequency (rf) magnetic

TABLE I. Time settings t_1 to t_5 and t_{extr} in ms to define the start of rf power and duration of counting as used in the experiments (see Fig. 3).

Isotope	t_1	t_2	t_3	t_4	t_5	Δt_2	Δt_4	t_{extr}
^{39}Ca	190	250	942	997	2900	697	1903	200
^{37}K	190	250	1100	1150	2900	843	1749	200
^{35}K	40	100	230	280	2500	130	320	50

field perpendicular to B_0 was used [10]. This rf magnetic field B_1 was produced by means of a powerful adjustable LCR circuit with two coils placed on each side of the stopper crystal (see insert of Fig. 2).

In addition to the setup shown in Fig. 2, a 70% Ge detector was positioned laterally between the pole pieces of the magnet at a distance of 60 mm from the center of the stopper crystal. The Ge detector used for estimating the purity of the implanted beam by recording β -delayed γ radiation had an efficiency of 0.64(2)% at 661 keV.

III. MEASUREMENTS AND EXPERIMENTAL RESULTS

In order to derive the nuclear polarization P from the measured up-to-down positron emission ratios, the well-known expression for the β^+ -decay angular distribution $W(\theta)$ can be used:

$$W(\theta) = 1 + (v/c)AP\cos(\theta),$$

where θ is the angle between the emitted positron relative to the spin axis of the parent nucleus, v/c is the positron velocity divided by the speed of light ($v/c \approx 1$ for high-energy β

particles), and A denotes the asymmetry parameter of the decay which can be derived from β -decay theory [11].

The telescopes detected positrons emitted in an interval of θ angles, with $\theta=0^\circ$ corresponding to the axis of the static field. The mean value $\eta = \overline{\cos\theta}$ was determined with static field giving the counting rates $U \propto 1 + AP\eta$ and $D \propto 1 - AP\eta$ for the upper and lower telescopes, respectively. The loss in detection efficiency caused by the helix-like trajectories of the positrons in the magnetic field was estimated with a Monte Carlo simulation. Assuming spherically symmetric emission of positrons with momentum distribution shapes corresponding to allowed decays, $\eta = 0.64(1)$ is obtained for ^{37}K with $E_\beta^{\text{max}} = 5127$ keV. For ^{39}Ca , the same η value was obtained. It can be compared with the estimate $\eta = 0.63(1)$ given in Ref. [9] for a comparable detection apparatus.

The up-to-down ratio R is given by

$$R = G \frac{1 + AP\eta}{1 - AP\eta},$$

with G including asymmetries of the implantation and the detector system. Performing a similar measurement after reversing the spins gives

$$R' = G \frac{1 - AP\eta}{1 + AP\eta}.$$

By forming the double ratio R/R' the experimental asymmetries cancel.

Our measurements were performed in a sequence of implantation, rf application, and β counting as depicted in Fig. 3. In the beam-off periods between consecutive spills, first the ratio R and then the ratio R' were measured. In the next

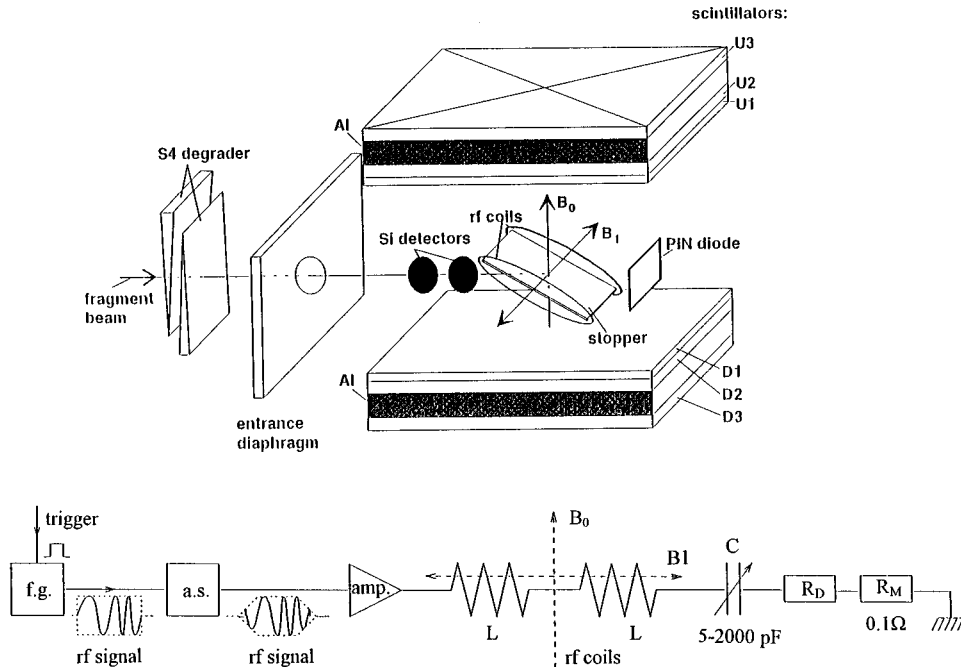


FIG. 2. β detectors in the static field B_0 perpendicular to the rf field B_1 . For $^{35,37}\text{K}$ fragments a KBr stopper, for ^{39}Ca fragments a CaF_2 stopper was used. Insert: radio frequency (rf) circuit with adjustable capacitor C , coil inductance L , damping resistor R_D and for monitoring R_M is connected to a power amplifier ENI A500 (amp), a self-constructed amplitude shaper (a.s.) and a function generator HP 33120A (f.g.). The trigger signal is provided by a time sequencer (see Fig. 3).

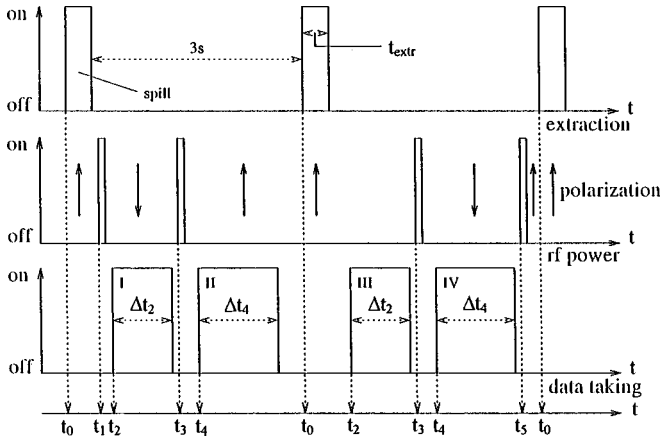


FIG. 3. Time schedule of the experiment: the collection of fragments is done during SIS spills, the rf application and data acquisition in beam-off periods. The distance of the subsequent spills is 3 s. The extraction time t_{extr} is adjusted to the half-lives of the fragments and is 200 ms and 50 ms, timing signals t_1 to t_5 were delivered by time sequencers. Values are given in Table I, t_0 is provided by the SIS synchrotron. In resonance, the spin polarization is reversed.

counting period, the polarization directions were inverted and the ratios R' and R were obtained. Each of the double ratios R/R' and R'/R can be used to derive the polarization. In cases with high counting statistics, the fourfold ratio can also be used [9].

A. The polarization of ^{37}K

The ^{37}K fragments were stopped in a KBr single crystal. Table I lists the fragment collection, rf-power application, and positron measurement timing schedule used. Because of the lower positron energy in ^{37}K decay, only the two innermost scintillator telescope members (U1-U2 and D1-D2, respectively) could be used (see Fig. 2). For this purpose, the trigger condition was defined as

$$((U1 \wedge U2) \wedge \overline{U3}) \vee ((D1 \wedge D2) \wedge \overline{D3}).$$

The anticoincidence conditions $\overline{U3}$ and $\overline{D3}$ suppressed the background from cosmic radiation to a level of 10%. By requiring the coincidences $U1 \wedge U2$ and $D1 \wedge D2$, the effect of PM noise was effectively reduced. The detection threshold was ≈ 0.5 MeV. The ground state of ^{37}K has $I^\pi = 3/2^+$ and decays with a half-life of $t_{1/2} = 1226(7)$ ms and Q value $Q_{\text{EC}} = 6148.5(15)$ keV [12]. The main decay branch (98.1%) is the mixed Gamow-Teller and Fermi transition ($I^\pi = 3/2^+ \rightarrow I^\pi = 3/2^+, T = 1/2$) to the ground state of the daughter nucleus ^{37}Ar . For this transition, the asymmetry parameter $A(^{37}\text{K}) = -0.55(2)$ was given by [9].

For each of two primary beam inclination angle settings, $+7.5$ mrad and -8.5 mrad, measurements were made for four different bins of the fragment longitudinal momentum distribution. The up-to-down ratios R and R' obtained in the time intervals I, II, III, and IV, as defined in Fig. 3, are listed in Table II. From the product $AP\eta$, obtained by forming fourfold ratios (see previous section), the polarization P could be derived. In Fig. 4, the resultant polarization values are plotted as a function of fragment longitudinal momen-

tum. While changing the incident beam direction reverses the sign of the polarization, the absolute value of $P \approx 1.5\%$ is comparable for both angles. It is also notable that the polarization does not change sign when scanning the longitudinal fragment momentum and that its magnitude is nearly constant over the whole momentum range. (Possibly the largest effect is obtained when the fragment velocity matches that of the incident projectile.) The result is discussed in detail in Sec. V.

B. The polarization of ^{39}Ca

The ^{39}Ca fragments were stopped in a CaF_2 single crystal. The trigger condition was identical to that used for the case of ^{37}K and the timing was similar (see Table I). The ^{39}Ca ground state has $I^\pi = 3/2^+$ and decays exclusively to the $3/2^+$ ground state of the daughter nucleus ^{39}Ar , with $t_{1/2} = 859.6(14)$ ms and $Q_{\text{EC}} = 6530.6(18)$ keV [12]. For this mixed Gamow-Teller and Fermi decay, the empirical asymmetry parameter $A(^{39}\text{Ca}) = 0.83(2)$ was given [9].

While keeping the primary beam incidence angle constant at 7.5 mrad, four different fragment longitudinal momentum bins were investigated. By forming fourfold ratios of the up-to-down ratios measured at each setting, the corresponding polarization values P given in Fig. 5 were obtained. To check this, a measurement was performed with the rf field turned off. Within the experimental uncertainties, no polarization could be observed, allowing an upper limit of $P(^{39}\text{Ca}) < 0.3\%$. This ‘‘negative’’ result is discussed in Sec. V.

C. The g factor of ^{35}K

Prior to our experiment, the magnetic properties of ^{35}K were largely unknown. Our experiment, aimed at measuring the magnetic moment of this drip-line nucleus, should be seen as a first step towards an accurate determination of the ^{35}K g factor.

Motivated by the observation that the sign of the ^{37}K polarization was independent of the fragment longitudinal momentum, the FRS was set to simultaneously accept the full momentum distribution of ^{35}K fragments. The ^{35}K fragments were implanted into a KBr single crystal. The timing of implantation and measurements is given in Table I. In comparison to the other isotopes studied in this work, ^{35}K has a shorter half-life [$t_{1/2} = 190(30)$ ms [13]] and a larger Q value [$Q_{\text{EC}} = 11853(7)$ keV [12]]. The decay of the $I^\pi = 3/2^+$ ground state feeds ten levels in the daughter nucleus ^{35}Ar [12,13], the four most intense branches being indicated in Fig. 6. Because of its short half-life [$t_{1/2} = 1.775(4)$ s [12]], the decay of the daughter ^{35}Ar was disturbing the measurement. Because of the lower Q value of the contaminating decay [$Q_{\text{EC}}(^{35}\text{Ar}) = 5964.9(13)$ keV [12]], it was initially attempted to suppress its influence by selecting only the high-energy decay branches of ^{35}K by imposing the triple-coincidence trigger condition

$$(U1 \wedge U2 \wedge U3) \vee (D1 \wedge D2 \wedge D3).$$

However, with this condition the counting rate was very low and no polarization could be observed. This may be due to the decay branches, which have asymmetry parameters of

TABLE II. Polarization of ^{37}K observed at the tilting angles α of the ^{40}Ca beam.

α	+7.5 mrad			-8.5 mrad		
	$r_a - r_a$	$c_a - c_a$	$l_a - l_a$	$l_b - r_b$	$l_b - l_b$	$c_b - c_b$
R_I	1.0074(24)	0.9899(29)	1.0025(28)	1.0275(40)	0.9821(36)	1.0343(52)
R_{II}	1.0272(22)	1.0138(25)	1.0211(26)	1.0193(31)	0.9837(32)	1.0218(43)
R_{III}	1.0216(24)	1.0159(30)	1.0180(29)	1.0018(39)	0.9657(35)	1.0132(51)
R_{IV}	1.0243(22)	1.0033(25)	1.0124(26)	1.0317(32)	0.9845(32)	1.0367(44)
X	0.9834(44)	0.9643(52)	0.9765(52)	1.0381(72)	1.0177(70)	1.0357(96)
$AP\eta$ [%]	-0.21(6)	-0.45(7)	-0.30(7)	0.38(5)	0.22(9)	0.44(11)
P [%]	-0.60(17)	-1.28(20)	-0.85(20)	1.08(15)	0.63(26)	1.25(32)

^aThe momentum intervals as defined in Fig. 4.

opposite sign (see Fig. 6) and feed the low-lying levels of ^{35}Ar . If this is the case, emphasizing these branches might result in a very small effective asymmetry parameter.

In a second attempt, the trigger was relaxed to the double-coincidence condition used previously for ^{37}K and ^{39}Ca . This approach required correcting for the amount of ^{35}Ar decay-related counts in each of the four counting intervals I to IV. This could be achieved by fitting the experimental decay curves to find the contributions from ^{35}K decay and ^{35}Ar growth and decay, respectively. (The amount of ^{35}Ar remaining from previous spills was also taken into account.) The deduced net amount of ^{35}K is given in Table III. The applied fitting procedure required a more accurate ^{35}K half-life than the previously reported value 190(30) ms [13]. Using the Ge detector, it was possible to selectively measure the half-life of ^{35}K parallel to the positron counting. By selecting the 1750.6, 2589.8, and 2982.7 keV γ transitions [see Fig. 7(a)], the decay curve (δ) shown in Fig. 7(b) was obtained. After dead-time correction, curve (ϵ) was obtained, yielding the new value $t_{1/2}(^{35}\text{K}) = 178(8)$ ms. The dead-time correction was based on the recorded time behavior of the room background, 1460.8 keV γ ray from the decay of ^{40}K , the decay rate of which can be considered as constant.

Although the implantation rate of ^{35}K was much smaller than for ^{37}K and ^{39}Ca (the production cross section is estimated [14] to be two orders of magnitude smaller), the count rate in the positron telescopes was still high since the full

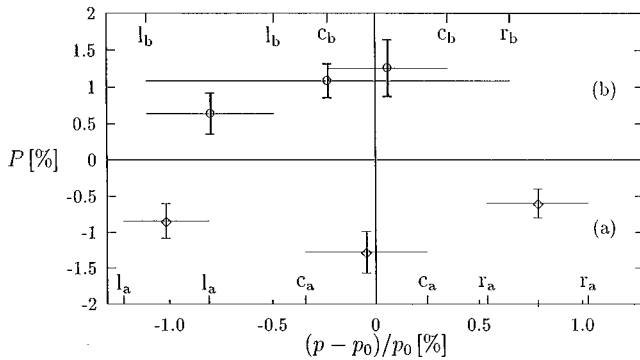


FIG. 4. Polarization of ^{37}K in fragmentation of 500 MeV/nucleon ^{40}Ca . (a) Tilting angle of primary beam on the target is $\alpha = +7.5$ mrad, (b) tilting angle $\alpha = -8.5$ mrad. The vertical bars represent 1σ statistical errors, the horizontal bars give the selected momentum bin of the GH distribution which has FWHM $(p - p_0)/p_0$ of $\sim 1\%$. The total time of measurement was 22 h.

fragment momentum distribution was accepted and because of the shorter half-life of ^{35}K . Indeed, the data acquisition suffered from very high dead times during the initial decay counting intervals (I and III in Fig. 2). Hence only data obtained during intervals II and IV were used for the determination of the g factor (see Table III).

Although the exact resonance frequency of ^{35}K is unknown, it can be estimated from, for example, shell model predictions of the g factor. The frequency of the variable rf magnetic field was swept over two slightly overlapping intervals (see Fig. 8). In the lower-frequency interval, a non-zero $AP\eta$ value was obtained, while the result of the higher-frequency scan is consistent with zero. Considering the overlap of the sweep ranges, the frequency interval in which spin reversal occurs is reduced, and the corresponding limits on the g factor of ^{35}K are deduced as

$$0.222(3) \leq g(^{35}\text{K}) \leq 0.252(4).$$

This experimental value, $g = 0.24(2)$, can be compared to different model predictions. While the classical Schmidt value [15] is $g_{\text{Schmidt}} = 0.083$, more recent shell model calculations give $g_{\text{Perez}} = 0.290$ [16] and $g_{\text{USD}} = 0.122$ [17]. The experimental result agrees best with the prediction by Brown *et al.* [17], made prior to the measurement, of $g_{\text{USD}}^{\text{eff}} = 0.243$. The g_{USD} values are based on the complete sd shell space wave functions and free nucleon g factors, and the $g_{\text{USD}}^{\text{eff}}$ values represent g factors derived with empirical “effective” operators [17]. Such effective g factors were found to be in good agreement with new experiments [17,18].

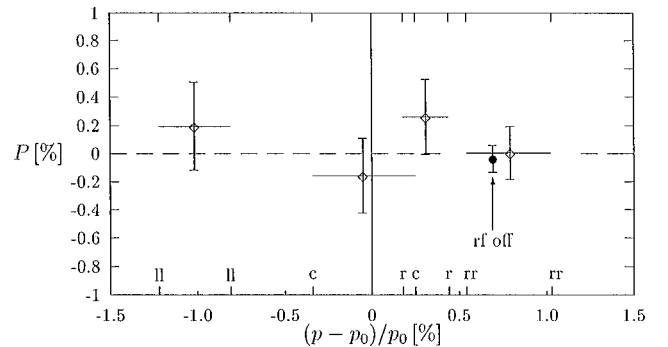


FIG. 5. Search for a polarization of ^{39}Ca . A tilting angle of $\alpha = +7.5$ mrad was used. Four selected momentum bins are indicated. The total duration of the measurement was 24 h.

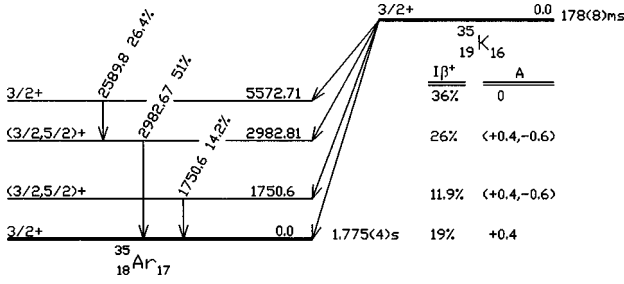


FIG. 6. Level scheme of ^{35}Ar . The main decay branches in ^{35}K decay are given with their branching being I_{β^+} and asymmetry parameters A . The ^{35}K half-life of the present work is given.

It should be noted that, since the sign of the asymmetry parameter A is unknown, the new result really corresponds to an *absolute* value of the g factor. Following the theoretical predictions, a positive sign has been adopted for the experimental value.

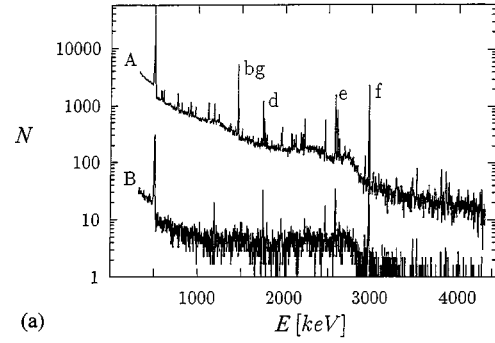
IV. g FACTORS OF MIRROR NUCLEI

While the magnetic moments of many $|T_z|=1/2$ nuclei are known in the light mass region up to $A=41$ [19], very little is known about the magnetic properties of $|T_z|=3/2$ nuclei. Only the values of ^9C and ^9Li are known, with $g(^9\text{C})=(-)0.9276(4)$ [4,20] and $g(^9\text{Li})=2.2927(4)$ [21] and of ^{13}O and ^{13}B , with $g(^{13}\text{O})=(-)0.9261(2)$ [20] and $g(^{13}\text{B})=2.1181(3)$ [22]. The new value for $g(^{35}\text{K})$ obtained in this work completes a new pair of $|T_z|=3/2$ moments, together with the g factor for ^{35}S , $g(^{35}\text{S})=0.667(30)$ [23].

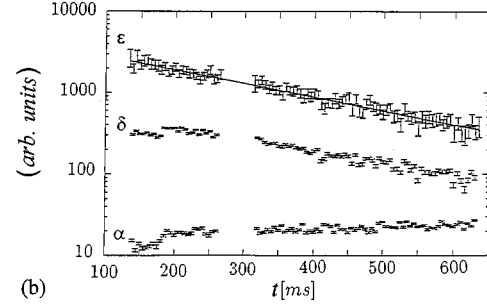
Within theoretical considerations (cf. for example [16]), isoscalar and isovector parts of the magnetic moments of mirror nuclei can be derived from experimental values, mainly for the isospin $|T_z|=1/2$ nuclei. Using the isoscalar momentum relation

$$\mu(T_z = -3/2) + \mu(T_z = +3/2) = J + (\mu_p + \mu_n - 1/2)\langle\sigma\rangle,$$

Matsuta *et al.* [4,20] derived the spin expectation value $\langle\sigma\rangle = 1.44$ for the ^9C - ^9Li pair and $\langle\sigma\rangle = 0.76$ for the ^{13}O - ^{13}B pair. The second value agrees with the results obtained from $|T_z|=1/2$ mirror nuclei in the very light mass region and the first value does not. The now available moments for the ^{35}K - ^{35}S mirror pair result in $\langle\sigma\rangle = -0.37(14)$, which corresponds well to the $\langle\sigma\rangle$ values obtained for $|T_z|=1/2$ nuclei



(a)



(b)

FIG. 7. (a) γ spectrum of ^{35}K measured with the 70% Ge detector during counting intervals (see Fig. 3). Spectrum A ungated, spectrum B in coincidence with β rays. The lines d,e,f of ^{35}K were used for the half-life measurement, line bg is the ^{40}K background. (b) Curve α is the time behavior of the bg line, curve δ the decay of ungated γ -ray lines d,e,f, and curve ϵ the corrected decay curve of ^{35}K .

in that mass region [4,20], e.g., $\langle\sigma\rangle = -0.27, -0.12, -0.40, -0.23$ for the mirror pair nuclei with $A = 33, 35, 37,$ and 39 , respectively.

In the odd-nucleon group model of Buck and Perez [16], the contribution from the even nucleon group is negligible because of pairing effects and the magnetic moments of an odd proton mirror nucleus and its odd-neutron partner can be expressed as

$$\mu_P \approx g_e^p J + (g_s^p - g_e^p) \cdot S_z$$

and

$$\mu_N \approx g_e^n J + (g_s^n - g_e^n) \cdot S_z,$$

TABLE III. Experimental values of the ^{35}K g -factor measurement. $U_{\text{II,IV}}, D_{\text{II,IV}}$ total number of double coincidences, $R_{\text{II}}, R_{\text{IV}}$ derived ratios and $AP\eta$ values (see text).

rf sweep	0.819 MHz–1.001 MHz		0.926 MHz–1.133 MHz	
	total	^{35}K fraction	total	^{35}K fraction
U_{II}	211 795	69.42(4)%	140 336	69.45(4)%
U_{IV}	212 797	69.03(4)%	140 404	69.48(4)%
D_{II}	208 085	67.39(4)%	136 616	67.86(4)%
D_{IV}	207 834	67.19(4)%	137 093	67.59(4)%
R_{II}	1.0178(32)	1.0301(34)	1.0272(40)	1.0513(42)
R_{IV}	1.0239(32)	1.0519(34)	1.0242(39)	1.0528(41)
$(AP\eta)_{\text{IV,II}}[\%]$	0.15(12)	0.52(12)	-0.07(14)	0.04(7)

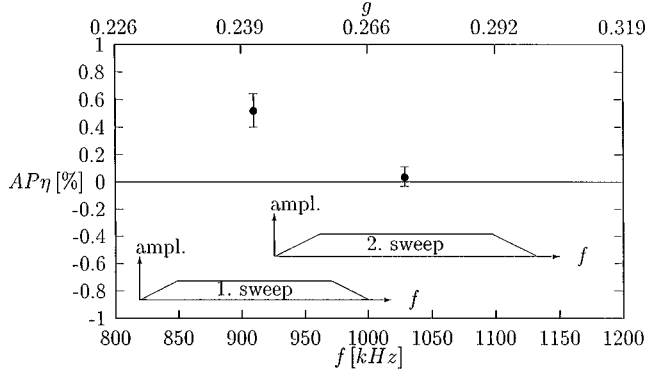


FIG. 8. Frequency intervals 1 and 2 used in the g -factor measurement of ^{35}K . The resonance with spin reversal is in the first interval (first sweep). The inserted blocks give the mixture of fr amplitudes as a function of frequency.

respectively, where g_e^p denotes the orbital g factors for protons and g_e^n that for neutrons. g_s^p and g_s^n are the respective spin g factors, J is the z component of the total angular momentum of the nucleus, and S_z is the total spin of the odd-nucleon group.

In the extreme case when only one odd nucleon is active, the expressions correspond to the classical Schmidt values which in general show very poor agreement with the experimental values.

The spin part of S_z could be excluded from the discussion by assuming a linear dependence between mirror pair magnetic moments [16]:

$$\mu_p = a\mu_N + bJ,$$

where the coefficients a and b are given by the $g_e^{p,n}$ and $g_s^{p,n}$ values.

Interestingly, the magnetic moments of the $|T_z|=1/2$ mirror nuclei follow this trend with the parameters $a = -1.145(12)$ and $b = 1.056(21)$ hardly differing from the free-nucleon values $a = -1.199$ and $b = 1$ [16].

The first $|T_z|=3/2$ pair, ^9Li - ^9C , does not agree with the linear dependence of the $|T_z|=1/2$ mirror nuclei [4]. The same is true for the magnetic moments of the $|T_z|=3/2$ nuclei ^{35}K - ^{35}S , and ^{13}B [22] and ^{13}O [20]. The three $|T_z|=3/2$ mirror pair magnetic moments cannot be described (within their experimental errors) by any other linear dependence either.

Since some deviations from the linear dependence defined by free-nucleon parameters have been discussed for $|T_z|=1/2$ nuclei [16], and still larger deviations may be expected for $|T_z|=3/2$ nuclei [4], it is very desirable to (i) more accurately determine the g factor for ^{35}K and (ii) determine the magnetic moments for further $|T_z|=3/2$ mirror pairs in order to check whether any linear dependence does exist for these nuclei.

V. POLARIZATION MODEL

We assume a projectile incident to be in the y direction and to collide peripherally with a target nucleus, and as a result the nucleons in the overlap volume are abraded from the projectile. In the models [1] and [2] for fragment polar-

ization, the angular momentum of the fragment is considered to be caused by the linear momentum of the internal Fermi motions of the abraded nucleons.

Vector $\vec{R} = (R_x, R_y, R_z)$ denotes the mean position of the abraded nucleons with respect to the center of the projectile and $\vec{k} = (k_x, k_y, k_z)$ denotes the Fermi momentum of the removed nucleons. The z axis is taken parallel to the vector of the scattering plane. In the rest frame of the projectile the angular momentum \vec{J} , which is transferred to the fragment, is then given by the expression

$$\vec{J} = -\vec{R} \times \vec{k}. \quad (1)$$

In peripheral abrasion the mean abrasion position may be $\vec{R} = (R_x, 0, 0)$ and a fragment polarization

$$P = \frac{J_z}{|\vec{J}|} = \frac{-R_x \cdot k_y}{|\vec{J}|} \quad (2)$$

results [1]. In a more detailed picture [2] the abrasion position is $\vec{R} = (R_x, R_y, 0)$. If so, the polarization of the fragment can be written as

$$P = \frac{-R_x \cdot k_y + R_y \cdot k_x}{|\vec{J}|}. \quad (3)$$

The essential argument of Okuno *et al.* [2] is that such a shift of the mean abrasion position in the y direction can be explained by an interaction of the nucleons removed from the projectile-target overlap volume with the remaining part of the projectile.

At small projectile energies the nuclear and Coulomb forces cause projectile deflections. Since trajectories of the fragments around the target nucleus to the left and right sides are distinguishable due to different deflections, a fragment polarization according to Eq. (2) was observed.

As the projectile energy increases, the deflection of the projectile in the reaction becomes smaller and smaller. At relativistic energies it is not possible to distinguish between the trajectories of the fragments having passed the target to the left or to the right side. Then, according to Eq. (2) the net polarization is zero.

However, if Eq. (3) applies, the net polarization does not vanish. For the abrasions taking place to the right or left of the projectile, the transferred angular momenta $R_y \cdot k_y$ do not cancel out.

A. Monte Carlo calculation

In order to study the effect proposed by Okuno *et al.* [2] we performed a simulation calculation. The fragmentation reaction is regarded as a two-step process. In the first step a peripheral collision between projectile and target, with subsequent interaction of the participating nucleons with the rest of the projectile, is considered. At the end of the first step an excited prefragment is formed. In the second step the deexcitation of the prefragment by particle evaporation is regarded.

For the simulation we have combined the Monte Carlo code of Okuno *et al.* [2] and the Monte Carlo code of

Gaimard and Schmidt [24]. The latter particle evaporation code is based on a model proposed by Campi and Hüfner [25].

1. Simulation of the first step

Projectile and target nucleus were regarded as spheres. For a given impact parameter b the overlap volume was calculated. The size of this volume corresponds to the number of abraded nucleons as proposed by Gosset *et al.* [26].

In the abrasion process individual nucleon-nucleon collisions between nucleons of the target and the projectile take place. Each of the nucleon-nucleon collisions was simulated separately. First, the position where the reaction takes place was chosen uniformly distributed in the overlap volume. Second, the momentum of the Fermi motion of a removed nucleon was chosen according to its probability distribution function $f(p)dp$, as $f(p) \propto p^2$ for $p \leq p_F$ and $f(p) = 0$ for $p > p_F$ where p_F denotes the Fermi momentum in the Fermi gas model of a nucleus. To simulate the directions of the nucleons after collision we adopted an isotropic nucleon-nucleon scattering process in the center-of-mass system of the two nucleons.

Each scattered nucleon traversed the projectile. The position of the first scattering in the overlap region and the direction of the scattered nucleon determine its path length d within the projectile nucleus. The probability W for the occurrence of a secondary scattering process was calculated from the equation

$$W = 1 - e^{-d/\lambda}, \quad (4)$$

where λ denotes the mean free path length of a nucleon in nuclear matter

$$\lambda = \frac{1}{\bar{\sigma}_{NN}\rho} B. \quad (5)$$

In this formula $\bar{\sigma}_{NN}$ is the average cross section for energy dependent nucleon-nucleon scattering [27,28] and ρ denotes the density of nuclear matter. The density was assumed to be constant. The factor B takes into account the Pauli blocking effect.

The secondary scattering of a nucleon with momentum and direction given in the first process was similarly calculated. This procedure was repeated until each of the participating nucleons had either left the projectile or had completed its scattering events within the projectile.

The total angular momentum \vec{J} of the prefragment is given by the sum of angular momenta transferred in i scatterings in the overlap volume and in the projectile volume:

$$\vec{J} = - \sum_i \vec{R}_i \times \vec{k}_i, \quad (6)$$

where \vec{R}_i and \vec{k}_i denote position and momentum of each removed nucleon.

The sum of momenta of the i removed nucleons and the momentum of the projectile determine the resultant fragment momentum:

$$\vec{P}_{\text{frag}} = \vec{P}_{\text{proj}} - \sum_i \vec{k}_i. \quad (7)$$

From these values, a deflection angle was obtained and it was checked whether the fragment entered the separator.

2. Simulation of the second step

The removal of a nucleon with momentum \vec{k} causes a heating of the prefragment. The excitation corresponds to the difference between Fermi momentum $|\vec{p}_F|$ and momentum $|\vec{k}|$. Thus, in the second step the evaporation of nucleons from the excited prefragment was calculated. No momentum transfer in evaporation was considered.

The probability distribution $P(A', Z')$ over the proton number Z' and the mass number A' of the prefragment were calculated from the corresponding numbers Z_p and A_p for the projectile as

$$P(A', Z') = \frac{\binom{Z_p}{z} \binom{A_p - Z_p}{a - z}}{\binom{A_p}{a}}, \quad (8)$$

in terms of the removed number of protons z , neutrons $a - z$, and nucleons a . The fragment distribution calculated with such a hypergeometrical ansatz is in good agreement with previous experimental data [24].

The simulation of the second step started with a prefragment with the mass A' , the proton number Z' , and the excitation energy E^* and ended when the fragment had reached the final parameters A_f , Z_f , and E_f .

In the code [29], the masses, level-density parameter, and excitation energy of the decaying nucleus and its daughter nucleus as well as the separation energies for p , n , and α decay were calculated. From these values, probabilities for the p , n , and α emission were derived and taken into account. The evaporation process was repeated until the remaining excitation energy was smaller than any separation energy. A detailed description of this evaporation model is given in [25] and [24].

B. Results of the simulation

A certain fragment can be produced via different mechanisms. Each production path is related to a specific polarization. Therefore, the observed polarization curve such as in Fig. 4 may be interpreted to be a superposition of different contributing curves. We found that the production of fragments which are two or more nucleons lighter than the projectile in nearly all the cases involves at least one evaporation step.

At medium projectile energies [2] the polarizations observed in various reactions were characterized by the width σ_Φ of the fragments' transverse deflection distribution (recoil of the nucleons' Fermi momenta), and the mean deflection angle $\bar{\theta}_{\text{def}}$, which is caused by the combined Coulomb and nuclear forces. The ratio

$$R = \frac{\bar{\theta}_{\text{def}}}{\sigma_{\Phi}} \quad (9)$$

approaches zero in the limit of very high projectile energies.

In this simulation we found that the ^{37}K is produced by $\approx 90\%$ via the following two mechanisms:

(i) Collision of ^{40}Ca projectile and ^9Be target with an impact parameter b_1 of nearly peripheral contact. Removal of one nucleon from the overlap volume and removal of one nucleon in a secondary scattering process within the projectile, followed by the evaporation of one nucleon from the prefragment ($\approx 47\%$).

(ii) Collision of the projectile and target with an impact parameter $b_2 < b_1$. Removal of two nucleons from the overlap volume, and subsequent evaporation of one nucleon ($\approx 43\%$).

The remaining 10% of ^{37}K productions is caused by a number of different mechanisms, e.g., the removal of three nucleons from the overlap volume without particle evaporation (1%) and the removal of one nucleon from the overlap volume and subsequent evaporation of two nucleons (4%).

We have considered only processes (i) and (ii). For the first one, a backshift of the abrasion position $R_{y,1} > 0$ resulted from the model calculation, and for the second one, the y component changed its sign, $R_{y,2} < 0$, and consequently the two polarization curves with $|R_{y,1}| < |R_{y,2}|$ partially cancel each other as shown in Fig. 9. The net polarization can be compared with the experimental result of Fig. 4. The size of the polarization is partly explained by this model. The calculation indicates that the width of the distribution curve of net polarization is somewhat smaller than that of the experimental curve, although we have already taken into account multiple scattering of the primary beam in the thick target.

It should be mentioned that in the earlier model [2] a scaling factor of $\sim 1/4$ was necessary to compare the calculation with experimental results.

The limitations of this model, like the assumption of constant nuclear matter density and neglect of other pro-

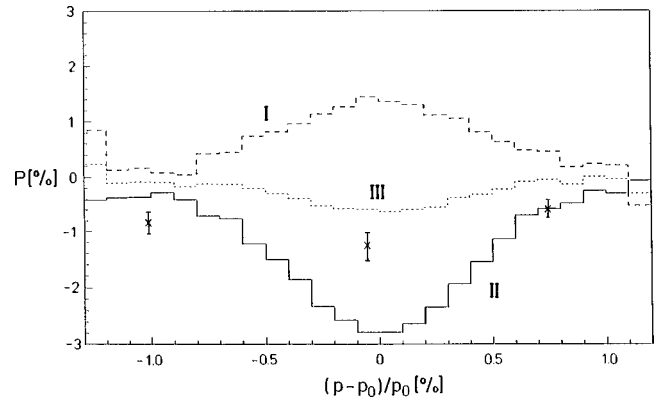


FIG. 9. Simulation calculation with a new polarization model at relativistic energies. Curves I and II correspond to the two main mechanisms of ^{37}K production in ^{40}Ca fragmentation (cf. text). Curve III is the weighted mean of curves I and II and gives the net polarization effect as a function of the longitudinal momentum. It is compared with the experimental values of Fig. 4(a).

cesses besides the nucleon-nucleon elastic scattering seem to affect the very peripheral collisions most. The simulation therefore might not apply to the one-neutron removal process from ^{40}Ca . It seems to be obvious, however, that the backshift of the mean abrasion position is small and therefore negligible polarization results, as was observed for ^{39}Ca .

We have also applied the model calculation to the production of other fragments and found that optimal polarization is expected for the abrasion of 3, 4, and 5 nucleons. When a still larger number of nucleons is removed, the polarization will not increase due to cancelling of the different contributing curves.

ACKNOWLEDGMENTS

One of us (M.H.) gratefully acknowledges support from the Alexander-von-Humboldt Foundation. This work was supported by the German Ministry of Research and Technology (BMFT) under contract No. 06GO667/TPHII.

-
- [1] K. Asahi *et al.*, Phys. Lett. B **251**, 488 (1990).
 [2] H. Okuno *et al.*, Phys. Lett. B **335**, 29 (1994).
 [3] H. Okuno *et al.*, Phys. Lett. B **354**, 41 (1995).
 [4] K. Matsuta *et al.*, Nucl. Phys. **A588**, 153c (1995).
 [5] W.-D. Schmidt-Ott *et al.*, Z. Phys. A **350**, 215 (1994).
 [6] M. Schäfer *et al.*, GSI Report 97-1, 39 (1997).
 [7] H. Geissel *et al.*, Nucl. Instrum. Methods Phys. Res. B **70**, 286 (1992).
 [8] T. Minamisono, J. W. Hugg, D. G. Mavis, T. K. Saylor, S. M. Lazarus, H. F. Glavish, and S. S. Hanna, Hyperfine Interact. **2**, 315 (1976).
 [9] K. Matsuta *et al.*, Phys. Lett. B **281**, 214 (1992).
 [10] A. Abragam, *Principles of Nuclear Magnetism* (Oxford University Press, Oxford, 1961).
 [11] H. Behrens and W. Bühring, *Electron Radial Wave functions and Nuclear Beta-decay* (Oxford University Press, Oxford, 1982), p. 218.
 [12] P. M. Endt, Nucl. Phys. **A521**, 1 (1990).
 [13] G. T. Ewan, E. Hagberg, J. C. Hardy, B. Jonson, S. Mattsson, P. Tidemand-Petersson, and I. S. Towner, Nucl. Phys. **A343**, 109 (1980).
 [14] K. Sümmerer, W. Brüche, D. J. Morrissey, M. Schädel, B. Szweryn, and Y. Weifan, Phys. Rev. C **42**, 2546 (1990).
 [15] Th. Schmidt, Z. Phys. **106**, 358 (1937).
 [16] S. M. Perez, Phys. Rev. C **36**, 1202 (1987); B. Buck and S. M. Perez, Phys. Rev. Lett. **50**, 1975 (1983).
 [17] B. A. Brown, W. Chung, and B. H. Wildenthal, Phys. Rev. C **22**, 774 (1980); B. A. Brown and B. H. Wildenthal, Nucl. Phys. **A474**, 290 (1987); B. A. Brown and B. H. Wildenthal, Annu. Rev. Nucl. Part. Sci. **38**, 29 (1988); B. A. Brown (private communication).
 [18] A. Klein *et al.*, Nucl. Phys. **A607**, 1 (1996).
 [19] P. Raghavan, At. Data Nucl. Data Tables **42**, 189 (1989).
 [20] K. Matsuta *et al.*, Hyperfine Interact. **97/98**, 519 (1996).

- [21] F. D. Correll, L. Madansky, R. A. Hardekopf, and J. W. Sunier, *Phys. Rev. C* **28**, 862 (1983).
- [22] R. L. Williams and L. Madansky, *Phys. Rev. C* **3**, 2149 (1971).
- [23] B. F. Burke, M. W. P. Strandberg, V. W. Cohen, and W. S. Koski, *Phys. Rev.* **93**, 193 (1954).
- [24] J. J. Gaimard and K.-H. Schmidt, *Nucl. Phys.* **A531**, 709 (1991).
- [25] X. Campi and J. Hüfner, *Phys. Rev. C* **24**, 2199 (1981).
- [26] J. Gosset, H. H. Gutbrod, W. G. Meyer, A. M. Poskanzer, A. Sandoval, R. Stock, and G. D. Westfall, *Phys. Rev. C* **16**, 629 (1977).
- [27] N. Metropolis, R. Bivins, M. Storm, A. Turkevich, J. M. Miller, and G. Friedlander, *Phys. Rev.* **110**, 185 (1958).
- [28] P. J. Karol, *Phys. Rev. C* **11**, 1203 (1975).
- [29] K.-H. Schmidt (private communication).